Predicting nonlinear properties of metamaterials from the linear response

Kevin O'Brien[1†], **Haim Suchowski**[1,2†], **Junsuk Rho**[1,2], **Alessandro Salandrino**[1], **Boubacar Kante**[1], **Xiaobo Yin**[1,2] and **Xiang Zhang**[1,2,3★]

The discovery of optical second harmonic generation in 1961 started modern nonlinear optics[1–3]. Soon after, R. C. Miller found empirically that the nonlinear susceptibility could be predicted from the linear susceptibilities. This important relation, known as Miller's Rule[4,5], allows a rapid determination of nonlinear susceptibilities from linear properties. In recent years, metamaterials, artificial materials that exhibit intriguing linear optical properties not found in natural materials[6], have shown novel nonlinear properties such as phase-mismatch-free nonlinear generation[7], new quasi-phase matching capabilities[8,9] and large nonlinear susceptibilities[8–10]. However, the understanding of nonlinear metamaterials is still in its infancy, with no general conclusion on the relationship between linear and nonlinear properties. The key question is then whether one can determine the nonlinear behaviour of these artificial materials from their exotic linear behaviour. Here, we show that the nonlinear oscillator model does not apply in general to nonlinear metamaterials. We show, instead, that it is possible to predict the relative nonlinear susceptibility of large classes of metamaterials using a more comprehensive nonlinear scattering theory, which allows efficient design of metamaterials with strong nonlinearity for important applications such as coherent Raman sensing, entangled photon generation and frequency conversion.

The broad applicability of Miller's rule, which holds for a wide variety of natural materials, stems from the fact that it is a direct result of the Lorentz oscillator description of material nonlinearity, in which a charge is moving in a non-quadratic potential[4]. An estimate for Miller's delta, the proportionality between the nonlinear and the linear susceptibilities, can be obtained by assuming that the linear and nonlinear restoring forces will be of similar magnitudes when the displacement of the charge is of the order of the inter-atomic distance, leading to an approximate value of Miller's delta of $\Delta_M \approx a^2/e$, where a is the inter-atomic distance and e is the electron charge. Experimentally, Miller's delta was found to be nearly constant, with a value of 0.45 ± 0.07 m² C⁻¹ for many semiconductor crystals, even though the linear and nonlinear susceptibilities spanned over four orders of magnitude[11,12]. Miller's rule was originally proposed for the transparency region of nonlinear crystals, where the losses were minimal, but was later extended to absorptive regions[13]. The model was shown to apply to a wide variety of materials, from semiconductor crystals to atomic vapours[14,15] and noble metals[16]. In a quantum mechanical treatment, the derivative of the potential is replaced with an average of the wavefunction over the ground state[17]. The development of metamaterials in the past decade allows the exploration of the nonlinear properties of such

materials at optical[18–23] and microwave[24] frequencies. Researchers have found that in some cases, such as the third harmonic emission from bow-tie and double-bar nanostructures[18,19], Miller's rule or its equivalent nonlinear oscillator model[25] fairly accurately predicts the nonlinear susceptibilities. However, the general validity of Miller's rule in optical metamaterials for arbitrary nonlinear processes, and specifically for second-order susceptibilities, is not known. Here we show experimentally that Miller's rule fails to describe the second-order susceptibility of metamaterials and predicts an incorrect optimum geometry for generating the highest second-order nonlinearity. We however demonstrate the optimal geometry can be correctly predicted with a more general nonlinear scattering theory. This general principle describes not only second-order but also higher-order nonlinear optical responses of plasmonic nanostructures over a broad wavelength range. The predictive capability of nonlinear scattering theory enables rapid design of optimal nonlinear nanostructures for sensing and integrated photonics.

Predicting the optimal metamaterial for nonlinear generation is a critical test of Miller's rule and microscopic theories of metamaterial nonlinearity. We have studied the second harmonic generation from metamaterial arrays in which the geometry varies gradually from a symmetric bar to an asymmetric shape (Fig. 1). A marked increase in the second-order susceptibility is expected owing to the extreme sensitivity of second harmonic generation to symmetry. Surprisingly, the nanostructure with the most obvious asymmetry, the highly curved U-shaped structure, does not yield the maximum second-order nonlinear susceptibility. Instead, the largest second harmonic emission is observed for an intermediate morphology. The transition between bar to U-shaped nanostructures—and thus the degree of asymmetry—is quantified by an asymmetry ratio, defined as the ratio of the vertical protrusion to the total length of the nanostructure. The asymmetry ratio varies from 0 to 0.3 along the horizontal axis of the array (Fig. 1), with a constant volume to avoid volume-dependent changes in the nonlinearity[26]. We study resonant and non-resonant interactions of the metamaterial with the pump pulse by varying the length of the nanostructure from 150 to 300 nm. This method allows us to separate the intrinsic variations in the metamaterial nonlinearities from the frequency-dependent linear and nonlinear susceptibility of the metal constituents[16]. The two-dimensional arrays of nanostructures are then illuminated at normal incidence with 200 fs laser pulses at 1,305 nm using confocal stage scanning microscopy. We find the maximum of the second harmonic emission for a specific geometry that corresponds to (length, ratio) = (292 nm, 0.18), as shown in Fig. 2a. In stark contrast, we find that the nonlinear oscillator model fails to predict the optimal nonlinear metamaterial, found to be at a much higher

[1]NSF Nanoscale Science and Engineering Center (NSEC), University of California, Berkeley 3112 Etcheverry Hall, UC Berkeley, California 94720, USA. [2]Materials Sciences Division, Lawrence Berkeley National Laboratory, 1 Cyclotron Road, Berkeley, California 94720, USA. [3]Kavli Energy NanoSciences Institute at the University of California Berkeley and the Lawrence Berkeley National Laboratory, Berkeley, California 94720, USA. [†]These authors contributed equally to this work. *e-mail: xiang@berkeley.edu
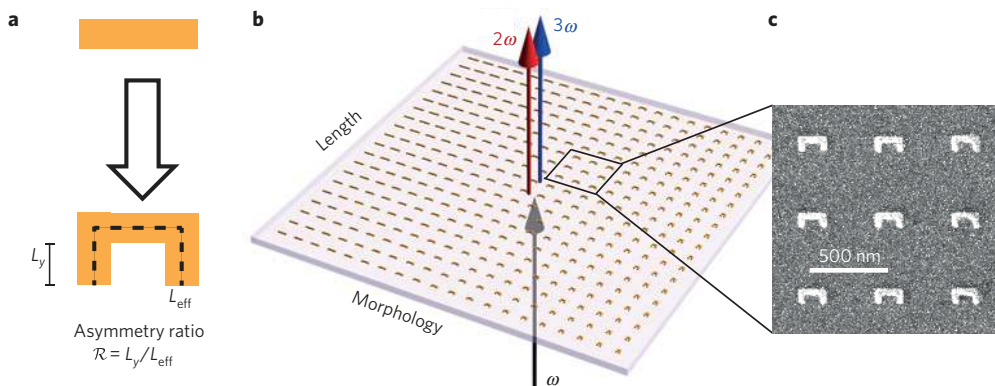
379

Figure 1 | Schematic of the metamaterial array. Nonlinear light generation from metamaterial arrays in which the geometry of the nanostructures varies gradually from a symmetric bar to an asymmetric U-shape. The second-order susceptibility is expected to be extremely sensitive to the symmetry of the metamaterial. **a**, Definition of the parameter space: the total length and asymmetry ratio of the nanostructures is changed throughout the array. Further details on the sample design are given in Supplementary Fig. 4. **b**, Schematic of the second and third harmonic generation as a function of the nanostructure length and morphology. A confocal microscope is used to excite the nanostructures with infrared laser pulses (1,305 nm). The nonlinear emission is measured in transmission and the linear transmission is characterized using a supercontinuum laser. **c**, Scanning electron microscope image of the nanostructures. To avoid particle–particle coupling, a period of 500 nm was used. This spectroscopy method allows us to separate the intrinsic variations in the nanostructure nonlinearities from the frequency-dependent linear and nonlinear susceptibility of the metal constituents.

ratio in the experiment (0.18 ± 0.02) than predicted by Miller's rule (0.12 ± 0.02), as seen in Fig. 2b. In addition, as seen in both models, the most asymmetric structures do not yield the highest second-order nonlinearity, as might be thought intuitively from simple spatial symmetry considerations. The optimum nonlinear metamaterial can be fully predicted by applying nonlinear scattering theory, which as we will show allows an accurate prediction of the correct far-field nonlinear susceptibility using the microscopic rather than the far-field linear response of the metamaterial.

Whereas the far-field linear response fails to predict the nonlinear properties of the metamaterial as Miller's rule prescribes, we find that the microscopic description can effectively predict the nonlinear susceptibility. In nonlinear scattering theory, the nonlinear emission is described by assuming a local nonlinear susceptibility tensor on the surface of the noble metal. This relationship can be quantified using the Lorentz reciprocity theorem[27] as

$$E_{nl}(2\omega) \propto \iint \chi_{nnn} E_n^2(\omega) \cdot E_n(2\omega) dS$$

where $E_{nl}(2\omega)$ is the nonlinear emission, χ_{nnn} is the local nonlinear susceptibility, and $E_n(\omega)$ and $E_n(2\omega)$ are the linear fields of the fundamental mode and the mode at the second harmonic frequency normal to the surface of the nanostructure. This process is illustrated schematically in Fig. 3a. The value of the overlap integral depends on the local field and the relative sign of the contributions: destructive interference between contributions can easily occur, resulting in low nonlinear emission. In contrast, good mode overlap, meaning constructive interference between the nonlinear polarization mode and its harmonics, will lead to very high far-field nonlinear emission, resulting in an intimate connection between the microscopic linear polarization and the far-field emission. By examining the microscopic origin of the far-field nonlinear emission, we can quantify this relationship and get an intuitive physical understanding of the violation of Miller's rule. In contrast, the numerical simulation using nonlinear scattering theory predicts an asymmetry ratio (~0.19) that is consistent with the experimental results, as shown in Fig. 2c.

The microscopic contributions, which are complex valued, add up from each region of the nanostructure, creating constructive or destructive interference in the far-field emission. A physically intuitive understanding of the net nonlinear emission in metamaterials can be obtained by plotting the value of $\mathbf{P} \cdot \mathbf{E}$ on a path around the nanostructure in a complex plane representation. The net nonlinear emission is proportional to the magnitude of the vector sum of the microscopic nonlinear sources. A large final magnitude corresponds to high nonlinear emission, which is a consequence of large polarizability and good overlap between the modes, whereas poor nonlinear emission can result from weak local fields as well as poor overlap or destructive interference between nonlinear generations in different regions. Four nanostructures with varying asymmetry ratios are plotted in Fig. 3b. For 'bar-like' nanostructures with a low asymmetry ratio (purple), the trajectory in the complex plane is not straight, illustrating the destructive interference of the microscopic nonlinear sources. In the opposite limit, for the greatest asymmetry ratio of 0.33 (dark green), the line integral follows a straight path in the complex plane, but the overall length of the vectors is smaller than the optimal nanostructure. The reason for this effect is the smaller absorption cross-section of the highly curved U-shaped structure than that of the bar. For the optimal nanostructure with an asymmetry ratio of 0.19 (brown), the path integral exhibits some curvature, but has the largest final radius. The optimal nanostructure for second harmonic emission represents a compromise between the absorption at the fundamental, the second harmonic, and the ability for the microscopic sources to combine constructively.

In the experiment, the second harmonic has a single peak along the vertical axis, indicating that the wavelength dependence is dominated by the resonance of one specific eigenmode at the fundamental frequency. To test the wavelength scaling, the nonlinear response was measured for different pump wavelengths. The second harmonic versus position on the array is shown in Fig. 4a–c for pump wavelengths of 1,160 nm, 1,220 nm and 1,305 nm, respectively. The relation between the position of the second harmonic emission peak and the excitation wavelength is linear (Fig. 4d), which corresponds to the linear relation between effective length and resonant wavelength. We find that, although the optimum length shifts with the pump wavelength, the optimum asymmetry ratio remains fixed. This optimum ratio depends on a delicate balance between the ability of the nanostructure to absorb light, which decreases roughly linearly with the length of the horizontal arm, and its ability to generate an asymmetric near-field current pattern, which depends on the length in the vertical direction (L_Y in Fig. 1). The constant
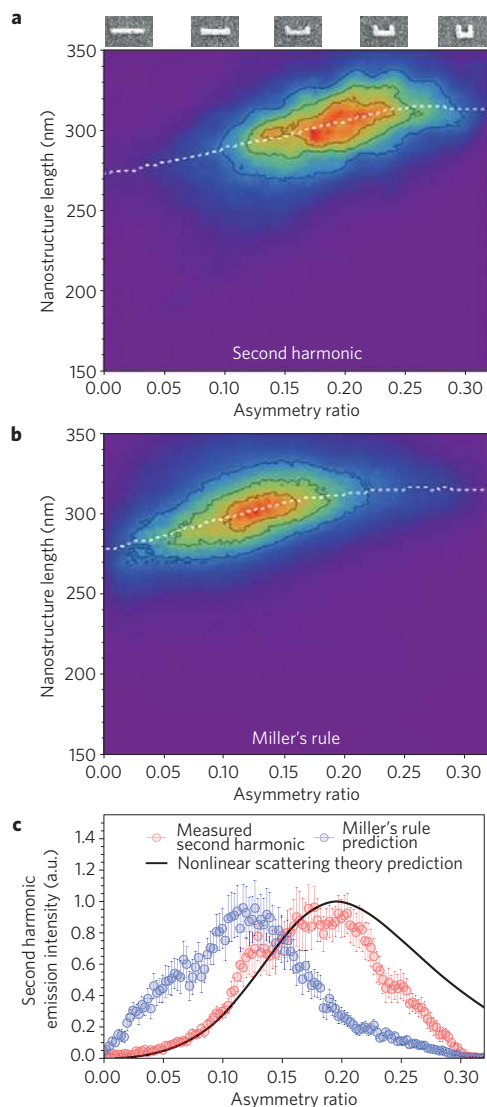
Figure 2 | Nonlinear scattering theory versus nonlinear oscillator model (Miller's rule). Experimental second harmonic emission for different geometries of nanostructure for $\lambda_{pump} = 1{,}305$ nm at normal incidence. Scanning electron microscope images of nanostructures with varying asymmetry ratios are shown above **a**. **a**, Experimental result for the second harmonic emission intensity (maximum in red and minimum in purple) as a function of the nanostructure length (y axis) and asymmetry ratio (x axis). **b**, Predicted second harmonic emission intensity following Miller's rule as a function of the nanostructure length and asymmetry ratio. From the transmission spectrum, we calculate the log of the transmission at the fundamental and second harmonic wavelengths, yielding a quantity proportional to the extinction cross-section. We then predict the relative nonlinear susceptibilities using Miller's rule, $\chi^{(2)}_{miller} \propto \sigma_{ext}(\omega)^2 \sigma_{ext}(2\omega)$. The white dashed lines in **a,b** indicate the nanostructure length with the highest second harmonic emission at a given asymmetry ratio. **c**, Second harmonic emission intensity as a function of the asymmetry ratio for three different cases, explained in the legend, with error bars indicating the standard deviation of the measured intensity. Miller's rule predicts a different optimum geometry from that seen in the experiment, whereas nonlinear scattering theory correctly predicts the optimum geometry.

relation that was observed in Fig. 4e suggests that such scalability will be valid also at different wavelengths as long as the linear relation between the resonance frequency and the length of the nanostructure holds. This conclusion adds considerable intuition to the design of nonlinear metamaterials.

There are some special cases where Miller's rule can serve as an approximation to guide the design of nonlinear nanostructures. One example is third-order nonlinearities, such as third harmonic generation, which do not have a symmetry-breaking requirement, so for dipole modes, the electric field and nonlinear polarization will add up constructively when integrated over the nanostructure. This eliminates one mechanism for the failure of Miller's rule. To demonstrate this, we have measured the third harmonic emission (Supplementary Fig. 7a) from the same array of nanostructures. The third harmonic generation was analysed in the same manner as done for the second harmonic case, that is, according to Miller's rule based on far-field polarizabilities. In the THG case, we find that Miller's rule (Supplementary Fig. 7c) predicts a similar dependence on geometry to that seen in the experiment. The implication of such a result is that the emission as a function of particle geometry can be reasonably described by the far-field radiation properties, largely because the third harmonic is a dipole-allowed process and the nonlinear polarization for such modes will add up constructively. This explains the good agreement that was achieved in earlier research on the nonlinear oscillator descriptions of experimental results for a wide range of geometries[18,19,28]. One small difference is that the far-field theory (Supplementary Fig. 7b) predicts a steeper drop in third harmonic intensity with the ratio than is observed in the experiment. The third harmonic emission from the U-shape is larger than expected from the nonlinear oscillator model owing to the enhanced local fields associated with the internal corners of the nanostructure as well as the changing ratio of absorption to scattering for the different structures[29].

In our present study, we have systematically studied the geometry dependence of metamaterial nonlinearity, demonstrating the validity of nonlinear scattering theory and thus the importance of the mode overlap between the nonlinear polarization and its harmonic modes for efficient nonlinear light emission. These experimental and theoretical methods can be used to calculate, predict and demonstrate other perturbative parametric processes, including multiple-wave mixing and parametric down-conversion in arbitrary nanostructures.

Methods

Sample preparation. The samples were prepared using a standard electron beam lithography (EBL) and metal lift-off process. The array of metamaterials is fabricated on top of a quartz substrate where a 2-nm-thick layer of indium–tin-oxide (ITO) is deposited by sputtering (Auto 306, Edwards) as an EBL conductive layer. After defining the nanometre scale metamaterial patterns in the bilayer photoresist with 250-nm-thick methyl methacrylate (MMA-EL8) and 40-nm-thick polymethyl methacrylate (PMMA-A2) with high-resolution EBL (CABL-9000C, Crestec), an electron beam evaporation system (Solution, CHA) is then used to deposit chromium and gold thin films, followed by gentle soaking in acetone to lift off the photoresist layer. The width of the nanostructures was approximately 40 nm, and the thicknesses of the gold and chromium were 35 nm and 2 nm, respectively. The chromium layer is used to enhance adhesion between the quartz surface and the gold layer.

Experimental method. A confocal microscope was used to measure the linear transmission and the nonlinear emission from each geometry. Stage scanning confocal microscopy allows us to investigate the geometry-dependent nonlinear properties of metamaterials, while avoiding the challenges associated with changing the laser wavelength, such as differences in pulse shape, focal volume size or transmission[30]. The light source is an optical parametric oscillator (Spectra Physics Opal) pumped by a $\sim$100 fs Ti:sapphire oscillator (Spectra Physics Tsunami). The pulse width is approximately 200 fs. The light source is focused to a spot size of 1.25 μm and scanned across the sample. A PMT is used for detection and colour filters are used to isolate the second and third harmonics. The filters were HG450/65 for the third harmonic and HG675/55 for the second harmonic. A KG3 filter was used to absorb the infrared. The power level was measured to be 100 μW of incident power at the back aperture of the objective. Spectral measurements show that at the power levels used no observable continuum emission is present. We work in transmission mode with a Zeiss LD-Plan-NEOFLUAR 63× 0.75 NA objective for excitation and a 40× 0.65 NA objective for collection. The collection half-angle for the objective is 40.5°.
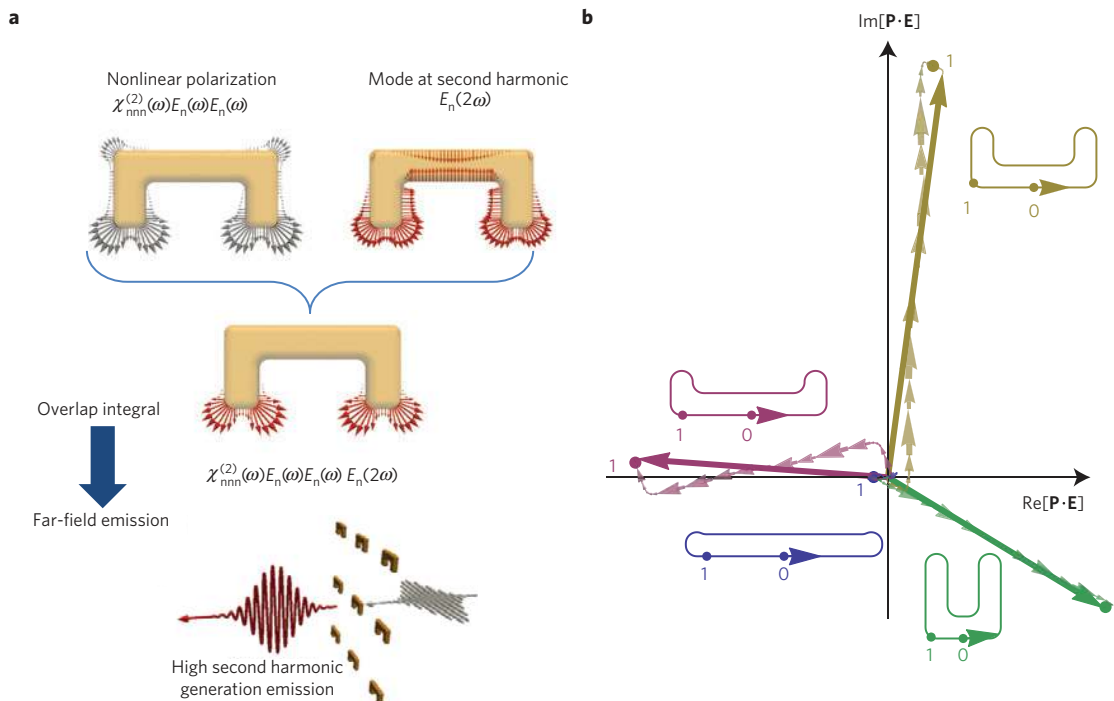
Figure 3 | Nonlinear scattering theory. a, The overlap integral of the microscopic nonlinear polarization, calculated from the linear fields at the fundamental frequency ω (for normal incidence), and the mode at the second harmonic yields the far-field nonlinear emission. **b,** Complex value of $\mathbf{P} \cdot \mathbf{E}$ plotted on a path around the nanostructure. The net nonlinear emission is proportional to the magnitude of the vector sum of the microscopic nonlinear sources. Four nanostructures with pulses of varying asymmetry are plotted in **b**.
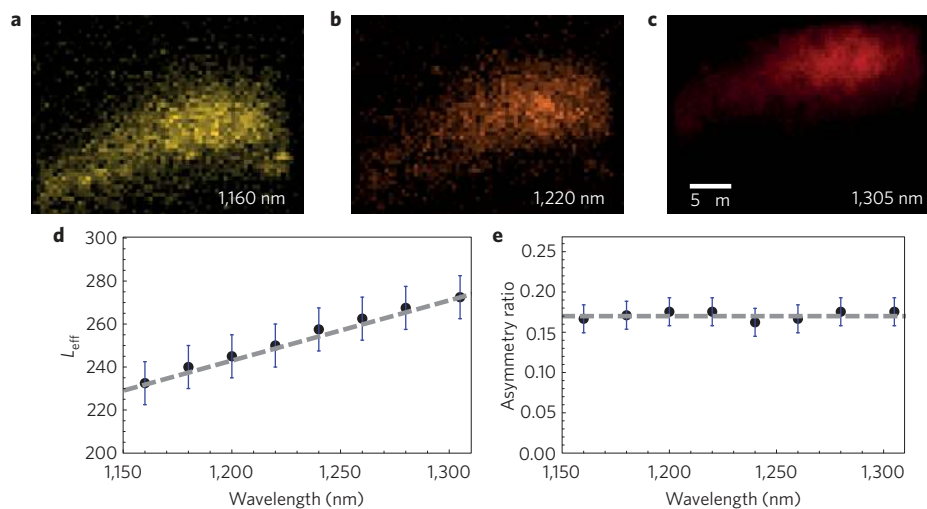

Figure 4 | Wavelength dependence of the optimal nanostructure for second harmonic generation. a–c, Spatial dependence of second harmonic generation for different excitation wavelengths. The same array of nanostructures is illuminated with pulses of varying wavelength, and the geometry that produces the maximum nonlinearity is determined. The vertical and horizontal axes represent the effective length and asymmetry ratio, respectively. **d,e,** Effective lengths (**d**) and asymmetry ratios (**e**) that produce the maximum amount of second harmonic as a function of the excitation wavelength. The optimum nanostructure length varies linearly with the wavelength, in agreement with the wavelength scaling of Maxwell's equations. The asymmetry ratio of the nanostructure that produces the maximum second harmonic remains fixed as the length is varied; illustrating the wavelength independence of the optimum asymmetry ratio. To determine the optimum geometry a centroid was fitted to the spatial maps of the second harmonic from the arrays of nanostructures. The grey dashed lines are a linear fit and the error bars indicate the standard deviation in fitting the centroid.

The detector is a Hamamatsu H7421-40 photon counting PMT. For linear transmission measurements we use a Fianium supercontinuum source. Experiments performed on sparse arrays (500 nm period) and for isolated nanostructures (2,000 nm period) yield similar results, suggesting that particle–particle and long-range interactions are not important in this system. Furthermore, the 1.25 µm focal spot illuminates of the order of only ten particles, limiting the interactions to a short range.

Simulation method. The linear and nonlinear response of each nanostructure was simulated using the finite-element solver COMSOL. A 600 nm diameter spherical domain with a perfectly matched layer (PML) was used. The geometry was rounded to a 5 nm radius of curvature. A uniform dielectric environment of $n = 1.3$ was used to account for the substrate and 2 nm ITO layer without introducing numerical instabilities. The simulations were performed for normal incidence. The reciprocity calculations were performed by first exciting the

nanostructure with a plane wave at the pump wavelength, then calculating the nonlinear polarization at every point on the nanostructure surface for the second harmonic and bulk for the third harmonic. Another simulation was then performed by sending in a second wave from the detector at the emission wavelength. The overlap integral was then performed, thus calculating the effective nonlinear susceptibility.

References

1. Franken, P. A., Hill, A. E., Peters, C. W. & Weinreich, G. Generation of optical harmonics. *Phys. Rev. Lett.* **7,** 118–119 (1961).
2. Armstrong, J. A., Bloembergen, N., Ducuing, J. & Pershan, P. S. Interactions between light waves in a nonlinear dielectric. *Phys. Rev.* **127,** 1918–1939 (1962).
3. Bloembergen, N. & Pershan, P. S. Light waves at the boundary of nonlinear media. *Phys. Rev.* **128,** 606–622 (1962).
4. Garrett, C. & Robinson, F. Miller's phenomenological rule for computing nonlinear susceptibilities. *IEEE J. Quantum Electron.* **2,** 328–329 (1966).
5. Miller, R. C. Optical second harmonic generation in piezoelectric crystals. *Appl. Phys. Lett.* **5,** 17–19 (1964).
6. Shalaev, V. M. Optical negative-index metamaterials. *Nature Photon.* **1,** 41–48 (2007).
7. Suchowski, H. *et al.* Phase mismatch-free nonlinear propagation in optical zero-index materials. *Science* **342,** 1223–1226 (2013).
8. Rose, A., Huang, D. & Smith, D. R. Controlling the second harmonic in a phase-matched negative-index metamaterial. *Phys. Rev. Lett.* **107,** 063902 (2011).
9. Rose, A., Larouche, S., Poutrina, E. & Smith, D. R. Nonlinear magnetoelectric metamaterials: Analysis and homogenization via a microscopic coupled-mode theory. *Phys. Rev. A* **86,** 033816 (2012).
10. Sukhorukov, A. A., Solntsev, A. S., Kruk, S. S., Neshev, D. N. & Kivshar, Y. S. Nonlinear coupled-mode theory for periodic plasmonic waveguides and metamaterials with loss and gain. *Opt. Lett.* **39,** 462–465 (2014).
11. Byer, R. L. Nonlinear optical phenomena and materials. *Annu. Rev. Mater. Sci.* **4,** 147–190 (1974).
12. Scandolo, S. & Bassani, F. Miller's rule and the static limit for second-harmonic generation. *Phys. Rev. B* **51,** 6928–6931 (1995).
13. Bell, M. I. Frequency dependence of Miller's rule for nonlinear susceptibilities. *Phys. Rev. B* **6,** 516–521 (1972).
14. Cataliotti, F. S., Fort, C., Hänsch, T. W., Inguscio, M. & Prevedelli, M. Electromagnetically induced transparency in cold free atoms: Test of a sum rule for nonlinear optics. *Phys. Rev. A* **56,** 2221–2224 (1997).
15. Miles, R. & Harris, S. Optical third-harmonic generation in alkali metal vapors. *IEEE J. Quantum Electron.* **9,** 470–484 (1973).
16. Matranga, C. & Guyot-Sionnest, P. Absolute intensity measurements of the optical second-harmonic response of metals from 0.9 to 2.5 eV. *J. Chem. Phys.* **115,** 9503–9512 (2001).
17. Rapapa, N. P. & Scandolo, S. Universal constraints for the third-harmonic generation susceptibility. *J. Phys. Condens. Matter* **8,** 6997–7004 (1996).
18. Hentschel, M., Utikal, T., Giessen, H. & Lippitz, M. Quantitative modeling of the third harmonic emission spectrum of plasmonic nanoantennas. *Nano Lett.* **12,** 3778–3782 (2012).
19. Metzger, B., Hentschel, M., Lippitz, M. & Giessen, H. Third-harmonic spectroscopy and modeling of the nonlinear response of plasmonic nanoantennas. *Opt. Lett.* **37,** 4741–4743 (2012).
20. Niesler, F. B. P., Feth, N., Linden, S. & Wegener, M. Second-harmonic optical spectroscopy on split-ring-resonator arrays. *Opt. Lett.* **36,** 1533–1535 (2011).
21. Canfield, B. K. *et al.* Local field asymmetry drives second-harmonic generation in noncentrosymmetric nanodimers. *Nano Lett.* **7,** 1251–1255 (2007).
22. Husu, H. *et al.* Metamaterials with tailored nonlinear optical response. *Nano Lett.* **12,** 673–677 (2012).
23. Dadap, J. I., Shan, J. & Heinz, T. F. Theory of optical second-harmonic generation from a sphere of centrosymmetric material: Small-particle limit. *J. Opt. Soc. Am. B* **21,** 1328–1347 (2004).
24. Poutrina, E., Huang, D., Urzhumov, Y. & Smith, D. R. Nonlinear oscillator metamaterial model: Numerical and experimental verification. *Opt. Express* **19,** 8312–8319 (2011).
25. Bassani, F. & Lucarini, V. General properties of optical harmonic generation from a simple oscillator model. *Nuovo Cimento D* **20,** 1117–1125 (1998).
26. Lippitz, M., van Dijk, M. A. & Orrit, M. Third-harmonic generation from single gold nanoparticles. *Nano Lett.* **5,** 799–802 (2005).
27. Roke, S., Bonn, M. & Petukhov, A. V. Nonlinear optical scattering: The concept of effective susceptibility. *Phys. Rev. B* **70,** 115106 (2004).
28. Gentile, M. *et al.* Investigation of the nonlinear optical properties of metamaterials by second harmonic generation. *Appl. Phys. B* **105,** 149–162 (2011).
29. Husnik, M. *et al.* Quantitative experimental determination of scattering and absorption cross-section spectra of individual optical metallic nanoantennas. *Phys. Rev. Lett.* **109,** 233902 (2012).
30. Castro-Lopez, M., Brinks, D., Sapienza, R. & van Hulst, N. F. Aluminum for nonlinear plasmonics: Resonance-driven polarized luminescence of Al, Ag, and Au nanoantennas. *Nano Lett.* **11,** 4674–4678 (2011).

Author contributions

K.O. and H.S. conducted the experiments. K.O. performed the theoretical calculations. J.R. fabricated the samples. K.O., H.S., X.Y. and X.Z. prepared the manuscript. X.Z. guided the research. All authors contributed to discussions.

Additional information

Supplementary information is available in the online version of the paper. Reprints and permissions information is available online at www.nature.com/reprints. Correspondence and requests for materials should be addressed to X.Z.

Competing financial interests

The authors declare no competing financial interests.